Research Article   **Open Access**

A Comparative Study of the Sintering Behavior of Pure and Iron-Substituted Hydroxyapatite

Erica Kramer, Michael Zilm and Mei Wei*

Department of Materials Science and Engineering, Institute of Materials Science, University of Connecticut, 97 North Eagleville Road, Storrs, CT 06269, USA

Abstract

Hydroxyapatite (HA) is a widely studied biomaterial for bone grafting and tissue engineering applications. The crystal structure of HA lends itself to a wide variety of substitutions, which allows for tailoring of material properties. Iron is of interest in ion substitution in HA due to its magnetic properties. The synthesis and characterization of iron-substituted hydroxyapatite (FeHA) have been widely studied, but there is a lack of studies on the sintering behaviors of FeHA materials compared to pure HA. Studying the sintering behavior of a substituted apatite provides information regarding how the substitution affects material characteristics such as stability and bulk mechanical properties, thereby providing insight into which applications are appropriate for the substituted material. In this study both pure HA and FeHA were synthesized, pressed into pellets, and then sintered at temperatures ranging from 900-1300°C and 600-1100°C, respectively. The study thoroughly examined the comparative sintering behaviors of the two materials using density measurements, mechanical testing, X-ray diffraction, and electron microscopy. It was found that FeHA is considerably less thermally stable than pure HA, with decomposition beginning around 1200°C for pure HA samples, while at 700°C for the FeHA. The FeHA also had a much lower mechanical strength than that of the pure HA. An *in vitro* cell culture study was conducted by immersing FeHA powder in cell culture media, with HA powder at equivalent doses as a control, verified that FeHA is a biocompatible material. Although the FeHA would be unsuitable for bulk applications, it is a potential material for a variety of biomedical applications including drug delivery, cancer hyperthermia, and bone tissue engineering composites.

Introduction

Hydroxyapatite (HA), being the main mineral phase of natural bone, is a commonly studied material for biomedical applications [1-3]. It is commonly used in bone grafting and tissue engineering applications due to its excellent biocompatibility and osteoconductivity [4]. HA, $Ca_{10}(PO_4)_6(OH)_2$, has a hexagonal crystal lattice structure [5], which allows for a wide variety of substitutions by anions, cations, and functional groups, such as the F- [6], $Fe^{2+/3+}$ [7-12], and CO_3^{2-} [13]. Iron is of interest as a substituted cation in HA due to the fact it is present naturally in trace amounts in both teeth and bone [8]. Additionally, its presence provides iron substituted apatite (FeHA) with possible magnetic properties that can potentially be applied to varied applications, including drug delivery, medical imaging, or hyperthermia based cancer therapies, for which pure HA is unsuitable [9,14-18]. The use of magnetic materials in these biomedical applications has the potential to greatly improve the prognosis for numerous patients suffering from a wide variety of diseases, but currently the most widely used magnetic nanoparticles for biomedical applications remain iron oxides. Unfortunately, safety is a constant concern when using these types of materials as toxicity and nondegradability limit their therapeutic efficiency [19]. Because HA is highly biocompatible and biodegradable, the application of HA with magnetic properties may minimize the current toxicity concerns in fields such as drug delivery, medical imaging, and cancer therapies.

Iron has been incorporated into the HA lattice during apatite synthesis, via controlled temperature and pH ion-exchange procedures, and via a simple room temperature ion exchange procedure with soaking time as short as 1 hour [7,9-12,20,21]. These procedures all resulted in powders with pure apatite crystal structure. All powders in which magnetic properties were measured also showed a change from the diamagnetism of pure HA to para- or super para-magnetic properties of iron substituted HA [9,12,20,21].

Clinically, the HA may be used in a variety of forms, including as a coating, as the reinforcement of a polymer-ceramic composite, and as a sintered ceramic. HA powder properties, such as crystallinity, surface area, and particle size, determine its effectiveness for specific applications. Additionally, powder properties and chemical composition affect HA sinterability [22]. During HA sintering reversible dehydroxylation occurs at all elevated temperatures yielding oxyhydroxyapatite, and occurs at a temperature generally above 1200°C [23,24]. Sometimes, the dehydroxylation of HA can occur as low as 800°C when impurities are present in the powder [24]. During the dehydroxylation process, HA decomposes to tricalcium phosphate (TCP) and CaO. This decomposition creates strain due to volume changes associated with the formation of new phases, and lowers the mechanical integrity of the sintered body [24].

Although some systematic studies regarding the sintering behavior of substituted apatites have been conducted, such as the work done by Kim et al. [25] and Qiu et al. [26], to the best of the authors' knowledge there has been little work conducted on the sintering behavior of FeHA.

Wang et al. did the report that iron containing HA nanoparticles calcined at temperatures well below 1000°C showed decomposition [8]. Additionally, work done by Morrissey et al. and Gross et al.

*Corresponding author: Mei Wei, Department of Materials Science and Engineering, Institute of Materials Science, University of Connecticut, 97 North Eagleville Road, Storrs, CT 06269, USA, Tel: (860) 486-9253; Fax: (860) 486-4745; E-mail: meiwei@engr.uconn.edu

[10,11] sintered FeHA with a pure apatite structure in air at 1150°C. After sintering at this temperature β-TCP and hematite phases were present [10,11] and the pellets displayed a brown to red color change accompanying the formation of the hematite phase [11]. The objective of this work was to provide an evaluation of the biocompatibility of FeHA powder, as well as a systematic study of the sintering behavior and corresponding mechanical properties of a series of temperatures, to determine the appropriateness of FeHA for biomedical applications.

Materials and Methods

Hydroxyapatite and iron-substituted hydroxyapatite synthesis

Hydroxyapatite powder was prepared via a wet precipitation procedure in which an aqueous solution of 2 g/dL ammonium phosphate (99+%, Acros) was added dropwise at a moderate dropping rate of about 75 drops per minute under vigorous stirring to a 2 g/dL aqueous calcium nitrate tetrahydrate (99%, Fisher) solution at 75°C. Ammonium hydroxide (~30%, Fisher) was also added to the mixed solution to bring up the pH to 11-12. After 3 hours of stirring at 75°C, the HA particles were collected by filtration and washed thoroughly with deionized water. The collected HA precipitates were dried at 90°C for 12-16 hours and ground by mortar and pestle into a fine powder. This resulting powder was then milled (SPEX 8000 Mixer/Mill) for 10 minutes in a steel canister with alumina milling balls.

Iron-substituted hydroxyapatite (FeHA) was produced using a simple ion exchange procedure [21]. HA powder, prepared as described above, was soaked in dilute ferric chloride solution (40% w/v, Fisher), at a concentration of 5 g/L, under moderate stirring for one hour, and then collected by filtration and washed thoroughly with deionized water. The powder was dried overnight and ground by mortar and pestle, and then SPEX milled for 10 minutes.

Pellet preparation and sintering

Milled HA and FeHA powders were uniaxially pressed into pellets using a bench top laboratory press (Carver Model C). For each pellet, 0.35 g of powder was pressed into a 13 mm pellet die well lubricated with stearic acid (97%, Acros) in acetone (99.9%, J.T. Baker) at a pressure of 150 MPa for 10 seconds. This yielded pellets with a thickness of approximately 1.63 mm for HA and 1.60 mm for FeHA.

Pellets were sintered at a selection of temperatures (900, 1000, 1100, 1200, and 1300°C for HA samples, and 600, 700, 900, 1000, and 1100°C for FeHA samples) and soaked at peak temperature for 2 hours in a chamber furnace (MXI model Z14) in air. Lower sintering temperatures were selected for the FeHA samples because initial results for samples run at the same temperatures as pure HA indicated that decomposition began for FeHA at temperature below 900°C. Samples were heated to the soaking temperature at a ramp rate of 5°C/min and allowed to cool naturally within the furnace to room temperature. A total of 10 pellets of each type of powder were sintered for each temperature point investigated.

Sample characterization

Starting powder characterization: FeHA powder synthesized using the procedure described above was thoroughly characterized and reported in our previous work [21]. The SPEX milled pure HA and FeHA powders were also examined via a JEOL JSM 6335F Field Emission Scanning Electron Microscope (FESEM) prior to pressing into pellets. The powder was dispersed in ethanol, sonicated for 20 minutes to reduce agglomeration, dried on a copper Transmission Electron Microscopy (TEM) grid, and sputter coated with gold palladium for 1 minute prior to imaging with an accelerating voltage of 10 kV. Sintered HA and FeHA pellets were then characterized using a variety of techniques.

Density and biaxial flexural strength: Density measurements were performed on green and sintered pellets using an Ohaus digital balance accurate to 1 mg and a caliper (Mitutoyo) accurate to 0.01 mm. Three diameters and three thickness measurements were taken for each pellet and the respective averages were used when calculating pellet density. A Tinius Olsen (150KS model) was used to determine the pellet biaxial flexure strength (modulus of rupture) on 13 mm diameter pellets using a 1000 N load cell at a crosshead speed of 0.01 mm/minute and a pin-on-disc test fixture set up per ASTM F 394 [27]. The Modulus of Rupture (MOR) was calculated based on the following equations:

$$S=-0.2387\ P(X-Y)/d^2 \qquad (1)$$

where S=maximum center tensile stress (MPa), P = total load causing fracture (N),

$$X = (1+\nu)\ ln[(B/C)^2] + [(1-\nu)/2](B/C)^2, \qquad (2)$$

$$Y = (1+\nu)[1+ln[(A/C)^2]] + (1-\nu)(A/C)^2, \qquad (3)$$

where ν=Poisson's ratio, 0.27, A=radius of support circle (mm), B=radius of loaded area or pin tip (mm), C = radius of specimen (mm), and d=specimen thickness at point of fracture (mm).

XRD characterization: As-prepared HA and FeHA, and those sintered at different temperatures were examined for phase purity and crystal structure using a Bruker D2 Phaser X-ray diffractometer (XRD) with a copper target, and voltage and current conditions of 40 kV and 40 mA, respectively. Conditions used were a 0.02°2-theta step size and a scan speed of 4°/min with a 2-theta range of 10-60.

FESEM characterization: Field Emission Scanning Electron Microscopy (FESEM) was used to examine the polished surface morphology and cross-section morphology of sintered pellets with an accelerating voltage of 10 kV. To observe the surface morphology of the pellets, the samples were polished using 1200/P4000 grit sandpaper for 3 minutes at 150 rpm, and then for an additional 20 minutes at 100 rpm using polishing cloth and 1 μm diamond paste. Polished pellets were then sputter coated with gold palladium for 1 minute prior to imaging. Pellet cross-sections were left unpolished and sputter coated with gold palladium for 1 minute prior to imaging.

Cell culture studies: Mouse calvaria 3T3-E1 cells were used to assess the biocompatibility of iron substituted hydroxyapatite (FeHA). Cells were grown in alpha modified eagle's medium (α-MEM) supplemented with 10% fetal bovine serum (Cellgro, FBS) and 1% penicillin-streptomycin under an atmosphere of 5% CO_2 at 37°C. At 90% confluence, cells were harvested and seeded at a density of 2×10^4 cells per well in a 24 well plate. Four hours were allotted for cell attachment after which the medium was changed to medium containing particles dispersed at concentrations of 20 μg/ml or 50 μg/ml HA or FeHA. Powders were sterilized by immersion in 70% ethanol for 30 minutes while under sonication. The powders were collected by centrifugation and rinsed with sterile filtered DIW three times and re-dispersed in supplemented α-MEM. Cellular proliferation was assessed at 1,3 and 7 days via alamar blue assay. In brief, cells were rinsed with phosphate buffer saline and the medium was refreshed with 1 ml of powder-free medium. Alamar blue was added at 1/10th the medium volume and incubated at 37°C for 4 hours. Aliquots, 200 μl, were taken

from each specimen in triplicates and the absorbance was measured at 570 and 600 nm. The percent reduction in alamar blue was calculated by:

$$Percent\ Reduced = (A_{570} - RoA_{600})*100$$

Results

Starting powder characterization

As was reported in our previous work, using a ferric chloride solution and a simple soaking procedure a phase pure FeHA material can be achieved in which iron substitutes into cation-exchange sites in the apatite crystal lattice replacing calcium ions. This material was thoroughly characterized using methods including XRD, energy dispersive X-ray spectroscopy (EDX), inductively couple plasma atomic emission spectroscopy (ICP-AES), Fourier Transform Infrared Spectroscopy (FT-IR), and Vibrating Sample Magnetometer (VSM) and Superconductive Quantum Interference Device (SQUID) analysis [21]. These previous results showed that after iron substitution the powder retained characteristic apatite crystal structure and functional groups, but the iron doped samples displayed paramagnetic properties, as opposed to the diamagnetism of pure HA. The effect of soaking time on iron content was also examined, and collectively X-ray diffraction and inductively coupled plasma atomic emission spectroscopy results suggested that an increase in soaking time led to an increase in iron content in the sample powder. An increase in iron content resulted in a decrease in sample crystallinity and a decrease in crystal lattice parameters. For a 1-hour soaking, such as used in this study, there were 0.064 g Fe/g FeHA, as measured by ICP-AES [21].

In this study, the starting powder was SPEX milled, and then characterized using FESEM. The FESEM images of the SPEX milled pure HA and FeHA samples in Figure 1 indicate that after SPEX milling pure HA for 10 minutes there is a wide particle size distribution ranging from about 30-300 nm length rod shaped particles. After ion exchange and an additional 10 minutes of SPEX milling the resulting particle morphology is mostly spherical shaped particles less than 100 nm in diameter.

Density and biaxial flexural strength

Both green and sintered density measurements were performed on HA and FeHA pellet samples. Ten pellets per sintering temperature were measured for both types of powders, and the densities were recorded as the average values of these measurements. Both green and sintered densities are listed in Table 1 and Figure 2 shows the sintered densities of both pellet types (HA and FeHA) as a function of sintering temperature.

The average green density of HA pellets was 1.65 g/cm³ and the average green density of FeHA pellets was 1.71 g/cm³. Table 1 summarizes the thickness, diameter, and density measurements of the HA and FeHA pellets sintered at different temperatures. For HA, the sintered densities increased with sintering temperature up to a maximum density of 2.92 g/cm³ at 1200°C, and then dropped at 1300°C. The peak density achieved was 93% the theoretical density of HA. For FeHA, sintered densities also increased with sintering temperature up to a point, before dropping. The highest density, 2.15 g/cm³, was achieved at 1000°C. There is a decrease in diameter with an increase in sintering temperature for every sample measured with the exception of the HA pellets sintered at 1300°C, and also a decrease in thickness compared to the green pellets for every sample measured with the exception of the HA pellets sintered at 1300°C and the FeHA pellets sintered at 1100°C. The FeHA pellets sintered at 1100°C experience a greater than 100% increase in thickness as compared to the FeHA pellets sintered at 1000°C.

After pellet densities were measured, the pellets were subjected to a modulus of rupture (MOR) test to study mechanical properties of the
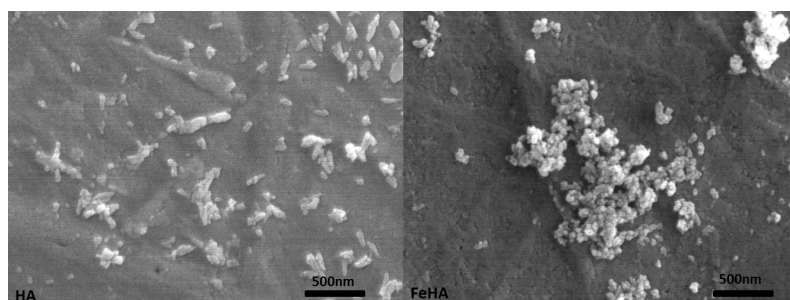
Figure 1: FESEM micrographs of SPEX milled HA and FeHA powders.

Sample	Avg. Green Diameter (mm)	Avg. Green Thickness (mm)	Avg. Green Density (g/cm3)	Avg. Sintered Diameter (mm)	Avg. Sintered Thickness (mm)	Avg. Sintered Density (g/cm3)	Avg. Sintered MOR (MPa)
HA 900°C	12.81	1.63	1.65	10.66	1.43	2.50	36.50
HA 1000°C				10.33	1.38	2.73	56.50
HA 1100°C				10.23	1.34	2.86	54.34
HA 1200°C				10.17	1.33	2.92	50.41
HA 1300°C				10.21	1.37	2.80	29.13
FeHA 600°C	12.78	1.60	1.71	12.38	1.56	1.70	7.38
FeHA 700°C				12.30	1.51	1.70	7.85
FeHA 900°C				12.00	1.47	1.78	8.92
FeHA 1000°C				10.93	1.43	2.15	16.87
FeHA 1100°C				10.91	2.94	1.06	4.43

Table 1: Diameter, thickness, and density measurements of sample pellets before and after sintering, and MOR of sintered pellets.

sintered pellets. The results of the MOR test are summarized in Table 1 and Figure 3. The values are presented as averages plus/minus standard deviations.

The MOR of the sintered HA samples ranged from the lowest value of 29.13 MPa for pellets sintered at 1300°C to a peak value of 56.50 MPa for pellets sintered at 1000°C. An ANOVA analysis was conducted on the mean MOR values resulting from 6 measurements per each of the 5 temperature points considered. This analysis resulted in a p-value of 2.89×10^{-5}, thus there is a significant difference ($p<0.05$) between the MOR values for the HA pellets sintered at different temperatures. The MOR of the FeHA sintered samples ranged from the lowest value of 4.43 MPa for pellets sintered at 1100°C to a peak value of 16.87 MPa for pellets sintered at 1000°C (as shown in Figure 3). An ANOVA analysis of these sample groups resulted in a p-value of 7.46×10^{-14}, thus there is also statistical significance between the MOR values for the FeHA pellets sintered at different temperatures. In addition to the MOR as a function of sintering temperature displayed in Figures 3 and 4 displays the MOR values for each pellet tested as a function of pellet density. Results for pure HA samples are shown in Figure 4a, and FeHA pellet results are displayed in Figure 4b.

XRD characterization

XRD analysis was used to examine the phase purity and crystal structure of the sintered pellets. The resulting XRD spectra for pure HA and FeHA samples are shown in Figures 5 and 6, respectively.

As is demonstrated clearly in Figure 5, the peaks present in each of the sintered samples are identical to those present in the un-sintered HA control spectrum. These peaks match well with the HA JCPD reference card 9-432. The figure shows that there is a small extraneous peak that
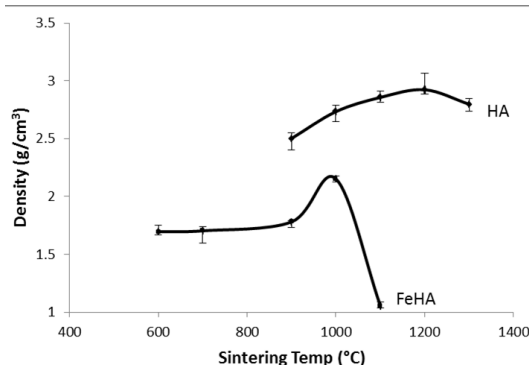

Figure 4: MOR as a function of density for (a) HA pellets and (b) FeHA pellets.

Figure 2: Post-sintered density of HA and FeHA sample pellets.
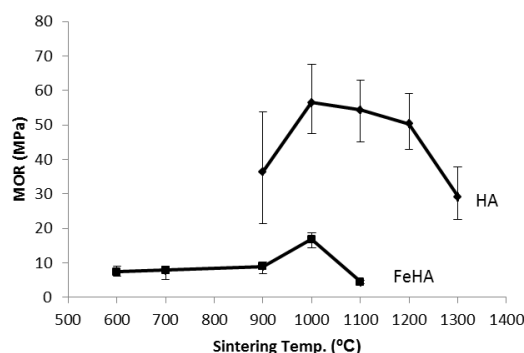
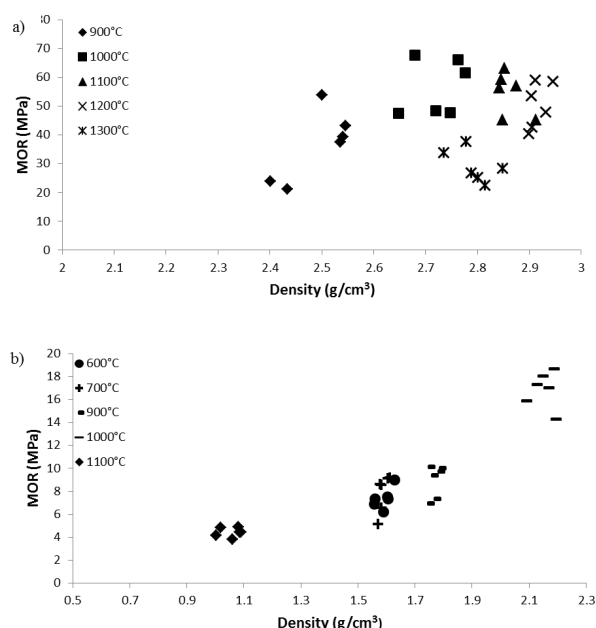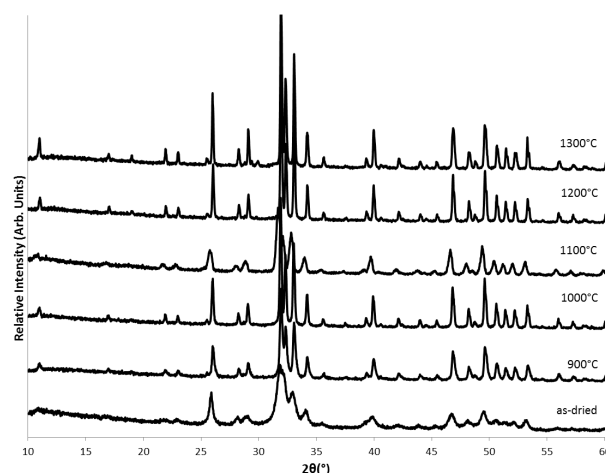**Figure 3:** Modulus of rupture averages for sintered HA and FeHA pellets.

Figure 5: XRD spectra for as-dried HA compared to HA sintered at 900°C, 1000°C, 1100°C, 1200°C, and 1300°C.

appears around 30° starting at 1200°C, which would match with the β-TCP peak at 29.68°2θ. Figure 6 shows that un-sintered FeHA results in pure apatite peaks matching with JCPD 9-432, although the broad peaks indicate that FeHA is more amorphous than un-substituted HA. FeHA sintered at 600°C also results in pure apatite peaks, but samples sintered at 700°C and above demonstrate the emergence of extraneous peaks, most notably at about 27.8°, 30.1°, 31.1° and 34.5°2θ. These peaks can be matched to β-TCP, which has significant characteristic peaks at 27.79°, 29.68°, 31.05° and 34.4°2θ, indicating that these samples are no longer phase pure hydroxyapatite. Another notable extraneous peak which begins to emerge in FeHA samples sintered at temperatures above 600°C, and becomes quite noticeable at 900°C, is at about 35.5°2θ. This peak is about one-third to one-half the relative intensity

of the TCP peak at 34.5°2θ, and can be assigned to an emerging iron oxide phase. In both HA and FeHA samples, sintering resulted in sharper XRD peaks, indicating an increase in crystallinity compared to the green pellets.
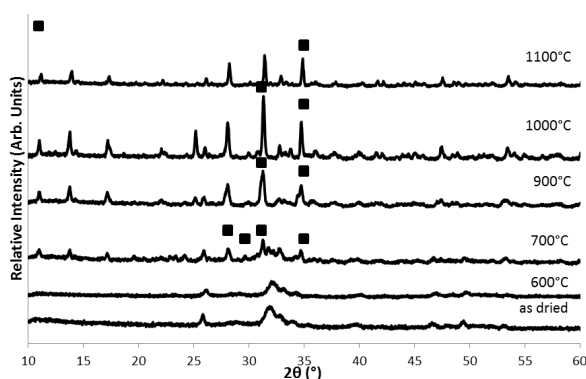
FESEM characterization

Unpolished fracture surfaces of the sintered pellets were imaged using FESEM allowing the microporosity of these samples and the extent to which the samples have been sintered to be examined. Figure 7 contains the micrographs of the HA pellet cross-sections sintered at different temperatures. It is apparent that at 900°C the pressed HA particles have not started to sinter yet. At 1000°C sintering has just started and there is a system of interconnected pores at the nanometer scale. The amount of sintering is increased at 1100°C, in which some

**Figure 6:** XRD spectra for FeHA compared to FeHA sintered at 600°C, 700°C, 900°C, 1000°C, and 1100°C.

areas are fully densified while some retain the interconnected porosity. The samples sintered at 1200°C are shown to be highly dense with discreet nanometer size pores. At 1300°C, as in the 1200°C, the HA particles seem fully sintered, but discreet pores around micron in size start to appear. Figure 8 contains the micrographs of the FeHA pellet cross-sections sintered at different temperatures. At 600 and 700°C, sintering has not begun in FeHA pellets, and the samples retain the interconnected microporosity seen in the HA samples sintered at 900°C. At 900°C sintering has begun but the interconnected microporosity is preserved and no area is fully sintered/densified. At 1000°C, the FeHA particles are essentially fully sintered and there are dense regions interspersed with micron scale pores. The level of porosity is greater than that seen in the HA sintered at 1200 and 1300°C. The micrograph of the FeHA sintered at 1100°C was taken on one of the walls in the pellets. This group of samples is fully dense and contains no microporosity.

FESEM images were also taken to examine the microstructure and porosity of the polished surface of the sintered pellets. The FESEM micrographs in Figure 9 depict that after sintering at each temperature point from 900-1300°C, the resulting microstructure of HA was dense pellets with pores in the micron range. At all sintering temperatures from 900°C up to 1300°C pores were comparable in size, up to about 10 μm. Pellets sintered at 900, 1000, and 1100°C show no obvious differences in microstructure or porosity. Pellets sintered at 1200°C have increased porosity as compared to the pellets sintered at lower temperatures. Pore number was greatest in the pellets sintered at 1300°C.

The FESEM micrographs in Figure 10 depict the polished FeHA pellets sintered at temperatures from 600-1100°C. The pellets sintered at 600 and 700°C exhibit many pores, indicating they are hardly densified. In the pellets sintered at 900 and 1000°C, they are relatively denser but still with many pores. The bottom two micrographs in Figure 10 show
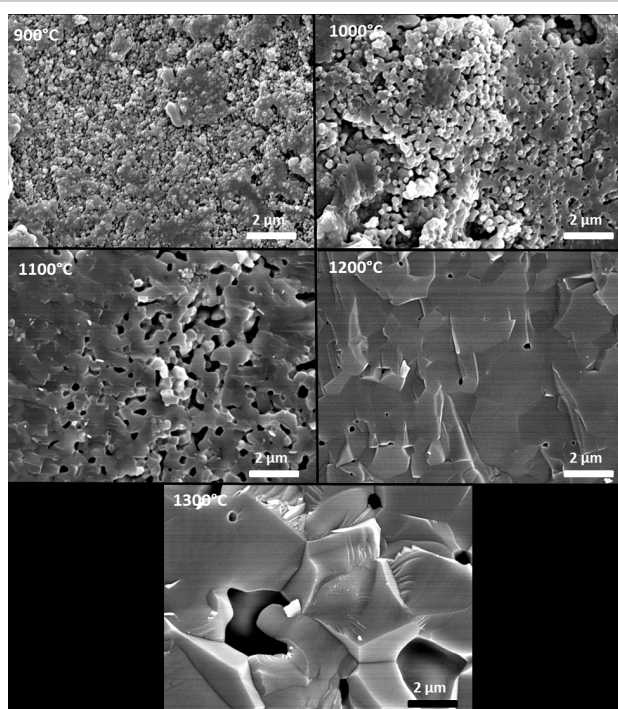
Figure 7: Cross sections of HA pellets sintered at 900°C, 1000°C, 1100°C, 1200°C, and 1300°C.
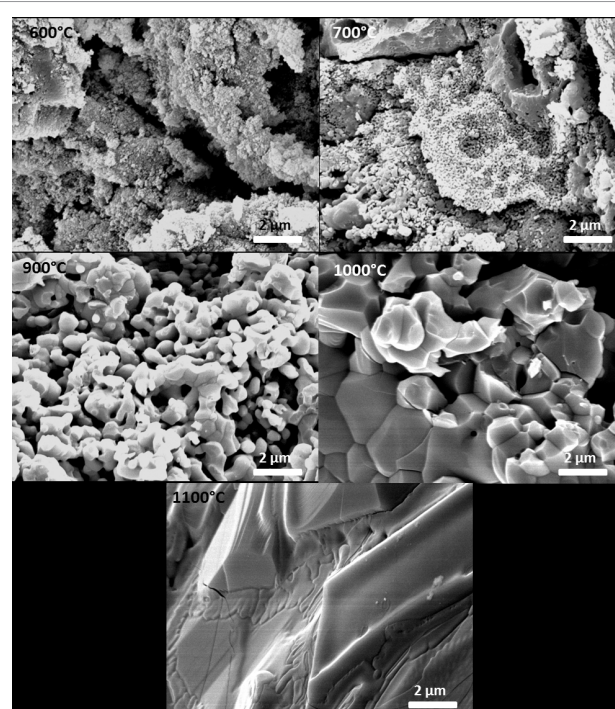
Figure 8: Cross sections of FeHA pellets sintered at 600°C, 700°C, 900°C, 1000°C, and 1100°C.
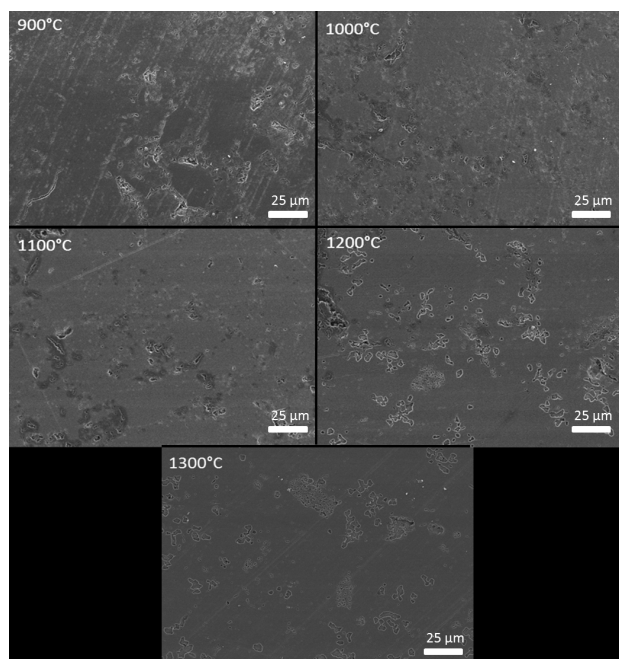
Figure 9: FESEM micrographs of polished HA pellets sintered at 900°C, 1000°C, 1100°C, 1200°C, and 1300°C.
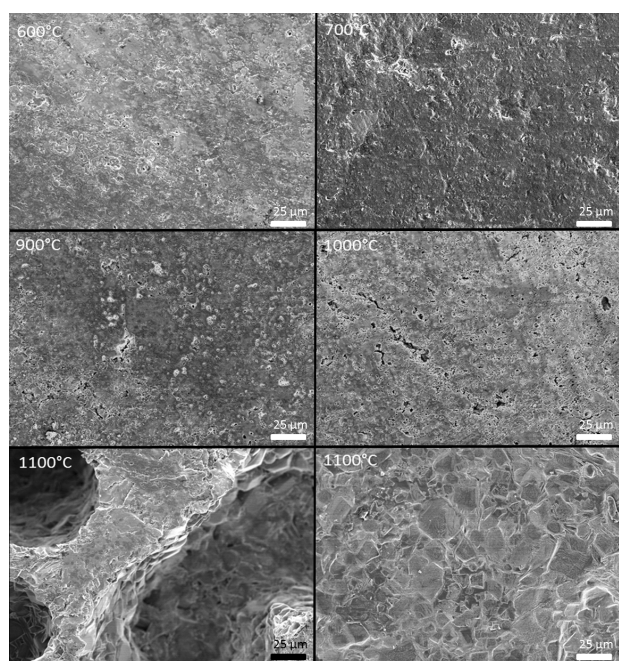
Figure 10: FESEM micrographs of polished FeHA pellets sintered at 600°C, 700°C, 900°C, 1000°C, and 1100°C (bottom left), and a micrograph of an unpolished FeHA pellet sintered at 1100°C with its outer shell intact (bottom right).

the microstructure of the FeHA pellets sintered at 1100°C, which is drastically different from any of the other microstructures observed at lower sintering temperatures. The pores in these pellets are at least an order of magnitude larger than the pores seen in the FeHA samples sintered at lower temperatures. The pores are separated by dense walls

that are tens of microns thick. The micrograph in which the outer shell of the FeHA pellet sintered at 1100°C was left intact shows that the shell structure of these samples is highly textured, and essentially completely dense. The FeHA sintered pellets exhibit distinctly different morphologies than the HA sintered pellets. The FeHA samples sintered at 600 and 700°C are less dense than any of the sintered HA samples. Fee pellets sintered at 900 and 1000°C have similar microstructures to those seen in the HA pellets sintered at 1100 and 1200°C, respectively. These samples are dense but with pores in the micron size range; however, the numbers of pores in these samples are higher than those in the HA samples sintered at 1100 and 1200°C or FeHA pellets sintered at lower temperatures (e.g. 600 or 700°C). The microstructure observed in the FeHA samples sintered at 1100°C is not only drastically different from any other FeHA samples, but it is significantly different from any microstructures observed in the HA samples sintered at any temperature as well.

Figure 11, which consists of a micrograph of a cross-section of a FeHA pellet sintered at 1100°C, further examines the unique structure of this particular sample group. It is apparent that the pellet consists of a dense shell of a few hundred microns thick enclosing a porous core. The microstructure of this core consists of pores that are hundreds of microns large separated by walls that are tens of microns thick. The pores are not interconnected.

Cell culture study

Biocompatibility of FeHA was assessed by monitoring the proliferation of MC3T3-E1 cells over the course of a week with the Alamar blue assay. Alamar blue monitors the metabolic activity of cells, which can be related to the number of cells present. Healthy cells readily take up and reduce the active ingredient resazurin and reduce it to resorufin; damaged cells can reduce resazurin but at a slower rate. Figure 12 illustrates the biocompatibility of FeHA relative to HA. Cell proliferation is inhibited from 1 to 3 days at higher administered dosages of sample powder, for both HA and FeHA. Over the course of 7 days cell viability with FeHA was comparable to HA when applied at the same dosage, and the viability of cells exposed to higher dosages of HA recovered to be comparable to the viability of cells exposed to lower HA dosages.
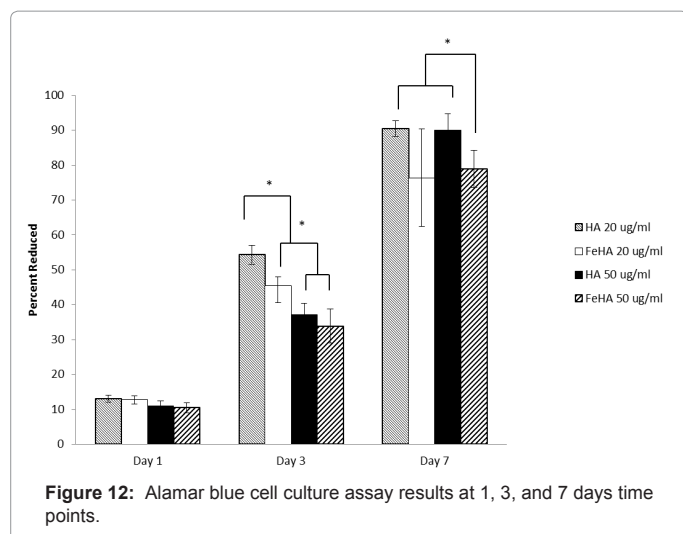
Discussion

In general, HA can be sintered up to 1200°C or above before it is decomposed to TCP and CaO [23,24]. In this study, HA was sintered
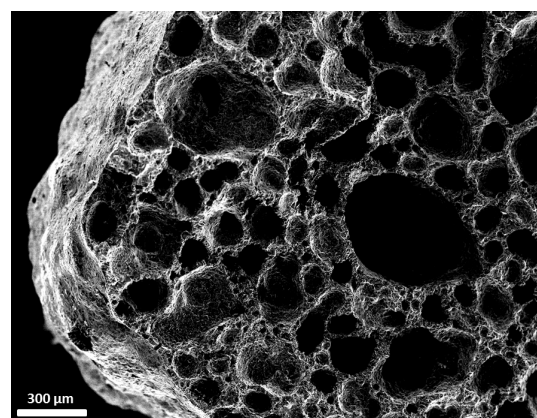

Figure 11: Cross-section of FeHA pellet sintered at 1100°C showing dense outer shell and highly porous interior of pellet.

Figure 12: Alamar blue cell culture assay results at 1, 3, and 7 days time points.

Figure 13: Photograph of FeHA pellets sintered at various temperatures.

from 900°C up to 1300°C. Ion substitution was also used to synthesize FeHA, an iron substituted material which maintains an apatite crystal structure but with magnetic properties [2]. The iron chloride ion exchange solution is acidic. Partial dissolution and re-precipitation of the HA particle surface helps facilitate the ionic substitution since the outer layer of the HA lattice in acidic conditions is loosely bound and calcium deficient. Previous work [21] indicated that the acidic soaking conditions did not have a significant impact on the particle morphology, suggesting HA particle dissolution was minimal. FeHA was sintered from 600°C up to 1100°C. The HA pellets underwent shrinkage (from an average diameter of 12.81 mm for the green pellets down to an average diameter of 10.17 mm for pellets sintered at 1200°C) but otherwise retained their white appearance with flat top and bottom surfaces. The FeHA pellets, on the other hand, underwent an obvious visual change upon sintering. As is seen in Figure 13, the un-sintered FeHA pellets were yellow. After being sintered at 600°C the FeHA was darkened, but remained yellow. The pellets sintered at 700°C developed a muddy brown color, which became redder up to 1000°C. Despite the distinct color changes present at the aforementioned temperatures the pellets retained the typical flat top and bottom surfaces that was seen in all of the pure HA samples, with shrinkage from 12.78 mm in diameter of the green pellets to 10.93 mm in the pellets sintered at 1000°C. However, the samples sintered at 1100°C changed drastically in appearance. These samples displayed a shiny outer shell with a dark metallic brown color. Upon breaking the pellets open, the inside was a matte dark brown color, with large pores visible to the naked eye. Additionally, although the pellet diameter shrank dramatically, the thickness increased significantly. As a combination of these two facts, the final density of the pellets actually dropped significantly compared to those sintered at 1000°C. It was also observed that both the top and bottom surfaces of the pellets became bumpy, as opposed to the flat surfaces that were observed at lower sintering temperatures for FeHA samples.

In addition to obvious visual differences between the pure HA pellets and the FeHA pellets, densification behavior and mechanical properties were also significantly different between the two material types. The initial green density of the FeHA pellets was higher than that of the pure HA pellets, 1.71 g/cm^3 as compared to 1.65 g/cm^3, as the starting FeHA powder was finer and easier to pack. Despite this higher initial density, the sintered densities of the FeHA pellets were considerably lower than those of the HA pellets. Although a
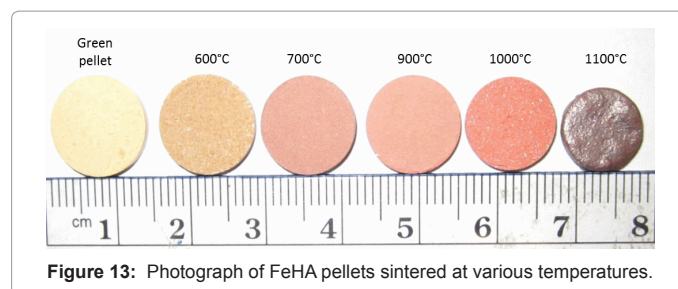
lower density is to be expected at lower sintering temperatures since densification typically increases with sintering temperature prior to the onset of decomposition [28], even when comparing FeHA and HA samples sintered at the same temperature the FeHA pellet densities are much lower. At their peak density, the HA pellets attain a density of 2.92 g/cm^3 sintered at 1200°C, which is 93% of the theoretical density of HA (3.156 g/cm^3). The density of FeHA on the other hand, never approaches the theoretical density of HA. It peaks at 1.91 g/cm^3, or 61% theoretical density, after sintering at 1000°C before decreasing drastically at higher temperatures.

The MOR of the FeHA pellets are also considerably lower than that of the HA pellets, which is unsurprising considering the lower densities observed for the FeHA pellets. The HA pellets achieve a high MOR value of 56.50 MPa, which compares favorably to the mechanical properties of bulk HA achieved by others in the literature [29,30] as well as the mechanical properties of natural bone, which has flexural modulus values ranging from 35 to 283 MPa, depending on factors such as patient age, overall health, and location in the body [31].

The MOR is displayed as a function of sintering temperature in Figure 2, and as a function of density in Figure 3 as well as Table 1. It is shown in Figure 2 that the MOR roughly plateaus between 1000 and 1100°C, with a slight decrease at 1200°C and a significant decrease (along with a decrease in density) at 1300°C. This may be due to the start of decomposition of HA to TCP at high temperatures (e.g. 1200 and 1300°C). The poor mechanical properties of the FeHA pellets may also be partially explained by decomposition of the HA to TCP and the formation of an iron oxide phase.

The FESEM images of polished sintered HA pellets (Figure 6) show a dramatic increase in porosity at 1300°C, corresponding to the decrease in density shown in Figure 1 and Table 1. The size of the micropores for the HA pellets sintered at 1300°C are also larger than those seen in the pellets sintered at 1200°C. This may be due to increased HA decomposition occurring at the higher temperature. Initially, sintering causes the close of pores and concurrently dehydroxylation results in the formation of an internal vapor pressure that exceeds the mechanical strength of the solid. This results in the formation of blowholes. At higher temperatures with the onset of decomposition a large amount of irreversible dehydroxylation occurs concurrently with decomposition, of which water vapor is a product, leading to a collapse of the hydrated HA structure, and a large increase in blowhole area [32].

The FeHA pellets were shown to have increased porosity from 900-1000°C (Figure 10) followed by a dramatic change in structure at 1100°C, corresponding with dramatic decreases in density and MOR at this temperature. At 1100°C the walls separating the large discreet pores in the FeHA pellet are seen to be fully dense with no microporosity. A dramatic phase change between 1000 and 1100°C may account for the drastic microstructural change observed. No such drastic change was seen at any of the studied temperature points in the HA pellets. The

core/shell structure seen in Figure 11, in which the pellets have a thin fully dense outer shell and a highly porous interior core, can likely be explained by the fact that the outside surface of the pellet is abundant in oxygen, forming a thick iron oxide layer which becomes the dense outer shell of the pellet. Then, as decomposition releases significant amounts of gas, the gas is trapped inside the pellet due to the dense shell, resulting in large pores observed in the FeHA pellets sintered at 1100°C.

It is clear from visual inspection, as well as density and mechanical property measurements, that the FeHA pellets have significantly different sintering behavior than the pure HA pellets. This is likely caused by the presence of iron ions in the HA lattice causing the reduced stability of the apatite crystal lattice and initiation of decomposition and formation of second phases at significantly lower temperatures than those which induce decomposition in pure HA. XRD analysis has confirmed this hypothesis.

A single-phase HA was achieved at sintering temperatures up to 1200°C, which was indicated by no extraneous peaks being present in the relative XRD spectra (Figure 5). Thermal stability up 1200°C is typical in pure HA [22,23]. Decomposition to β-TCP began at around 1200°C, as indicated by the emergence of a peak at 30° 2θ. The onset of decomposition explains the decrease in density and MOR in the HA pellets sintered at 1200 and 1300°C. The FeHA pellets were shown to be considerably less thermally stable than HA, and decomposition and the emergence of second phases started at temperatures as low as 700°C (Figure 6). In FeHA sintered at 700°C and above, extraneous peaks indicating the presence of TCP emerge at about 27.8°, 30.2°, 31.1° and 34.5° 2θ. There is also an extraneous peak observed at 35.5° with a relative intensity about one-third to one-half that of the β-TCP peak seen at 34.5° 2θ. The TCP reference peak at 34.4° has a relative intensity of 65, but HA and β-TCP peaks in the area of 35.5° (35.51° and 35.02°, respectively) each have low relative intensities of 6. The possibility should be investigated, therefore, that the peak located at 35.5° may come from a different second phase, most likely an iron oxide phase. In fact, magnetite (Fe_3O_4) and maghemite (γ-Fe_2O_3) are both possibilities. Each phase has a significant peak around 30° which may be overlapping with the β-TCP peak at that location. Additionally, the mineral magnetite has a peak at 35.45° with a relative intensity of 100 according to JCPD reference card 19-629 and maghemite has a peak at 35.66° with a relative intensity of 100 (JCPD 39-1346), either of which could potentially account for the extraneous peak seen at 35.5° in the spectra of the FeHA samples sintered above 700°C. Careful examination of the FeHA pellet spectra in Figure 5 shows that in pellets sintered at 900°C and above (Figure 5) a small peak is present at about 57.0° 2θ. Additionally, there is a small but obvious peak at 33.5° which is most prevalent in the FeHA sample sintered at 1000°C. Magnetite has a reference peak with a relative intensity of 30 at 56.99° and hematite (α-Fe_2O_3) has a reference peak with a relative intensity of 100 at 33.31° 2θ, therefore the sintered FeHA pellets likely contain a mixture of calcium phosphate (HA and TCP), α-Fe_2O_3 and Fe_3O_4 phases. The presence of the iron oxide phases would account for the color change seen in the sintered FeHA pellets as well. Hematite is often a red color whereas magnetite is a dark color. Based on the change in pellet appearance, as well as the XRD data we can conclude that FeHA pellets sintered at temperatures below 700°C in air contain pure apatite phase (and have a resultant yellow color due to the presence of iron ions), and samples sintered at higher temperatures undergo various phase transformations. Pellets sintered from 700-900°C contain a mixture of calcium phosphate phases (HA and TCP) and iron oxides, mostly in the form of hematite (resulting in reddish colored pellets) pellets

sintered at 1000°C contain calcium phosphate phases and a mixture of hematite and magnetite, and samples sintered at 1100°C mostly contain a mixture of calcium phosphate phases and magnetite (Fe_3O_4) (resulting in dark brown colored pellets).

The incorporation of iron ions into the hydroxyapatite lattice results in an FeHA material that is less stable than pure HA, as proven by their difference in sintering behavior. The FeHA selected for use in this study was soaked in the ion exchange solution for 1 hour, and as such had the lowest iron content of the powders studied in the author's previous work [21]. Because increasing iron content results in decreased lattice parameters and crystallinity, it can be hypothesized that with an increase in iron content, the differences in sintering behavior as compared to the pure HA would be even more dramatic. The low sinterability and low MOR of FeHA as compared to pure HA makes the FeHA unsuitable for bulk applications. It can, however, be useful in applications which call for biocompatible nanoparticles in a powder form. Cell culture studies indicated that there was no significant limitation in cell viability after 1 week of exposure to FeHA when compared to pure HA. The initial decrease in cell viability at days 1 and 3 may be due to the fact that although HA is biocompatible, some recent studies have shown that calcium phosphates can have an inhibitory effect on osteoblast *in vitro* [33-35]. Although *in vitro* cell culture studies are useful tools for initial-stage biological screening of biomaterials, behavior *in vivo* is completely different. Preliminary results of an ongoing *in vitro* degradation study being conducted by the authors suggest solubility of both FeHA and HA is minimal after 1 week, which was the maximum time point considered in the cell culture study presented in this work, and as such the different material solubilities should have a minimal influence on cell proliferation after 1 week. The lower stability of the FeHA material suggests that it may degrade in the body faster than pure HA, and later time points of *in vitro* degradation are being investigated for future publication. A faster degradation rate than that experienced by pure HA may be a desirable trait, depending on the specific application. Possible applications may include use as a drug delivery vehicle, for cancer hyperthermia, or as a filler in bone repair composites.

Conclusion

This study successfully examined the sintering behavior of magnetic, biodegradable FeHA nanoparticles in a systematic and thorough manner. HA was sintered to a maximum density of 2.92 g/cm³ and a peak MOR of 56.50 MPa. It did not begin to decompose until 1200°C. Sintering FeHA at temperatures as low as 700°C caused its decomposition into a multi-phase material containing HA, TCP, hematite, and magnetite. The maximum density and MOR achieved by FeHA were 2.15 g/cm³ and 16.87 MPa, respectively. It was discovered, through the use of density measurements, mechanical testing, FESEM, and XRD analysis, that FeHA has lower thermal stability than pure HA thus, it is expected that FeHA will degrade faster *in vivo* than pure HA. This fact, combined with material biocompatibility and the magnetic properties of FeHA suggest that it is suitable for applications which require fast biodegradable magnetic nanoparticles, such as drug delivery, hyperthermia treatments for cancer, or as a filler in bone repair composite.

References

1. Martini FH (2006) Fundamentals of Anatomy & Physiology : San Francisco: Pearson- Benjamin Cummings.

2. Weiner S, Wagner HD (1998) The Material Bone: Structure-Mechanical Function Relations. Annu Rev Mater Res 28: 271-298.

3. Park JB, Bronzino JD (2003) Biomaterials Principles and Applications. Boca Raton: CRC Press.

4. Elliot JC (1994) Structure and Chemistry of the Apatites and Other Calcium Orthophosphates. Elsevier Science, Netherlands.

5. Kay MI, Young RA (1964) Crystal Structure of Hydroxyapatite. Nature 204: 1050-1052.

6. Qu H, Vasiliev AV, Aindow M, Wei M (2005) Incorporation of Fluorine Ions in Hydroxyapatite by a pH Cycling Method. J Mater Sci Mater Med 16: 447-453.

7. Jiang M, Terra J, Rossi AM, Morales MA, BaggioSaitovitch EM, et al. (2002) Fe^{2+}/Fe^{3+} substitution in hydroxyapatite: Theory and experiment. Phys Rev B, Condens Matter Mater: Phys 66: 224-107.

8. Wang J, Nonami T, Yubata K (2008) Synthesis, structure and photophysical properties of iron containing hydroxyapatite prepared by a modified pseudo-body solution. J Mater Sci: Mater Med 19: 2663-2667.

9. Wu HA, Wang TW, Sun JS, Wang WH (2007) A novel Biomagnetic nanoparticle based on hydroxyapatite. Nanotechnology 18: 9.

10. Morrissey R, Rodriguez-Lorenzo LM, Gross KA (2005) Influence of ferrous iron incorporation on the structure of hydroxyapatite. J Mater Sci Mater Med 16: 387-392.

11. Gross KA, Jackson R, Cashion JD, Rodriguez-Lorenzo LM (2002) Iron Substituted Apatites: A Resorbable Biomaterial with Potential Magnetic Properties. Eur Cells Mater 3: 114-117.

12. Prakash KH, Kumar R, Ooi CP, Sritharan T, Cheang P, et al. (2006) Wet Chemical Synthesis and Magnetic Property Studies of Fe (III) Ion Substituted Hydroxyapatite. MCB 3: 177-178.

13. Cazalbou S, Eichert D, Ranz X, Drouet C, Combes C, et al. (2005) Ion exchanges in apatites for biomedical applications. J Mater Sci: Mater Med 16: 405-409.

14. Pankhurst QA, Connolly J, Jones SK, Dobson J (2003) Applications of magnetic nanoparticles in biomedicine. J Phys D: Appl Phys 36: R167-R181.

15. Duguet E, Vasseur S, Mornet S, Devoisselle JM (2006) Magnetic nanoparticles and their applications in medicine. Nanomedicine 1: 157-168.

16. Jain TK, Richey J, Strand M, Leslie-Pelecky DL, Flask CA, et al. (2008) Magnetic nanoparticles with dual functional properties: Drug delivery and magnetic resonance imaging. Biomaterials 29: 4012-4021.

17. Lu AH, Salabas EL, Schüth F (2007) Magnetic Nanoparticles: Synthesis, Protection, Functionalization, and Application. Angew Chem Int Ed 46: 1222-1244.

18. Gupta AK, Gupta M (2005) Synthesis and surface engineering of iron oxide nanoparticles for biomedical applications. Biomaterials 26: 3995-4021.

19. Markides H, Rotherham M, El Haj AJ (2012) Biocompatibility and Toxicity of Magnetic Nanoparticles in Regenerative Medicine. J Nanomater 2012: 614094.

20. Li Y, Nam CT, Ooi CP (2009) Iron(III) and manganese(II) substituted hydroxyapatite nanoparticles: characterization and cytotoxicity analysis. JPhys: Conf Ser 187: 012024.

21. Kramer ER, Morey AM, Staruch M, Suib SL, Jain M, et al. (2013) Synthesis and characterization of iron-substituted hydroxyapatite via a simple ion-exchange procedure. J Mater Sci 48: 665-673.

22. Gibson IR, Ke S, Best SM, Bonfield W (2001) Effect of powder characteristics on the sinterability of hydroxyapatite powders. J Mater Sci Mater Med 12: 163-171.

23. Ruys AJ, Sorrell CC, Brandwood A, Milthorpe BK (1995) Hydroxyapatite sintering characteristics: correlation with powder morphology by high resolution microscopy. J Mater Sci Lett 14: 744-747.

24. Finoli A, McKeef D, Gerlach J, Nettleship I (2010) Phase transformation behavior of hydroxyapatite foams subject to heat treatment. Biomed Mater 5: 015004.

25. Kim SR, Lee JH, Kim YT, Rui DH, Jung SJ, et al. (2003) Synthesis of Si, Mg substituted hydroxyapatites and their sintering behaviors. Biomaterials 24: 1389-1398.

26. Qiu ZY, Li G, Zhang YQ, Liu J, Hu W, et al. (2012) Fine structure analysis and sintering properties of Si-doped hydroxyapatite. Biomed Mater 7: 045009.

27. ASTM Standard F 394 (1996) Test Method for Biaxial Flexure Strength (Modulus of Rupture) of Ceramic Substrates. ASTM International, West Conshohocken, PA.

28. Reed JS (1995) Principles of Ceramic Processing. (2ndedn), John Wiley & Sons Inc, New York.

29. Pattanayak DK, Divya P, Upadyay S, Prasad RC, Bao BT, et al. (2005) Synthesis and Evaluation of Hydroxyapatite Ceramics. Trends Biomater Artif Organs 18: 87-92.

30. Pattanayak DK, Dash R, Prasad RC, Rao BT, Rama Mahan TR (2007) Synthesis and sintered properties evaluation of calcium phosphate ceramics. Mater SciEng C 27: 654-690.

31. An YH, Draughn RA (2000) Mechanical Testing of Bone and Bone-Implant Interface. Taylor & Francis Group.

32. Ruys AJ, Wei M, Sorrell CC, Dickson MR, Brandwood A, et al. (1995)Sintering effects on the strength of hydroxyapatite. Biomater 16: 409-415.

33. Chou YF, Huang W, Dunn JC, Miller TA, Wu BM (2005)The effect of biomimetic apatite structure on osteoblast viability, proliferation, and gene expression. Biomater 26: 285-295.

34. Nebe JB, Müller L, Lüthen F, Ewald A, Bergemann C, et al. (2008)Osteoblast response to biomimetically altered titanium surfaces. Acta biomaterialia 4: 1985-1995.

35. Oreffo ROC, Driessens FCM, Planell JA, Triffitt JT (2008) Growth and differentiation of human bone marrow osteoprogenitors on novel calcium phosphate cements. Biomater 19: 1845-1854.